ACS NANO

www.acsnano.org

ARTICLE

# Development of a Virtual Cell Model to Predict Cell Response to Substrate Topography

Tiam Heydari,[†] Maziar Heidari,[‡] Omid Mashinchian,[§,⊥] Michal Wojcik,[∥] Ke Xu,[∥,□] Matthew John Dalby,[#] Morteza Mahmoudi,[*,△,▽] and Mohammad Reza Ejtehadi[*,†]

[†]Department of Physics, Sharif University of Technology, Tehran, 11155-9161, Iran

[‡]Max Planck Institute for Polymer Research, Ackermannweg 10, 55128 Mainz, Germany

[§]Nestlé Institute of Health Sciences (NIHS), EPFL, Innovation Park, 1015 Lausanne, Switzerland

[⊥]Doctoral Program in Biotechnology and Bioengineering, Institute of Bioengineering, École Polytechnique Fédérale de Lausanne (EPFL), 1015 Lausanne, Switzerland

[∥]Department of Chemistry, University of California, Berkeley, California 94720, United States

[□]Division of Molecular Biophysics and Integrated Bioimaging, Lawrence Berkeley National Laboratory, Berkeley, California 94720, United States

[#]Centre for Cell Engineering, Institute of Molecular, Cell and Systems Biology, College of Medical Veterinary and Life Sciences, University of Glasgow, Joseph Black Building, Glasgow, G12 8QQ, U.K.

[△]Nanotechnology Research Center and Department of Nanotechnology, Faculty of Pharmacy, Tehran University of Medical Sciences, Tehran, 14155-6451, Iran

[▽]Department of Anesthesiology, Brigham and Women's Hospital, Harvard Medical School, Boston, Massachusetts 02115, United States

*S* *Supporting Information*

**ABSTRACT:** **Cells can sense and respond to changes in the topographical, chemical, and mechanical information in their environment. Engineered substrates are increasingly being developed that exploit these physical attributes to direct cell responses (most notably mesenchymal stem cells) and therefore control cell behavior toward desired applications. However, there are very few methods available for robust and accurate modeling that can predict cell behavior prior to experimental evaluations, and this typically means that many cell test iterations are needed to identify best material features. Here, we developed a unifying computational framework to create a multicomponent cell model, called the "virtual cell model" that has the capability to predict changes in whole cell and cell nucleus characteristics (in terms of shape, direction, and even chromatin conformation) on a range of cell substrates. Modeling data were correlated with cell culture experimental outcomes in order to confirm the applicability of the virtual cell model and demonstrating the ability to reflect the qualitative behavior of mesenchymal stem cells. This may provide a reliable, efficient, and fast high-throughput approach for the development of optimized substrates for a broad range of cellular applications including stem cell differentiation.**

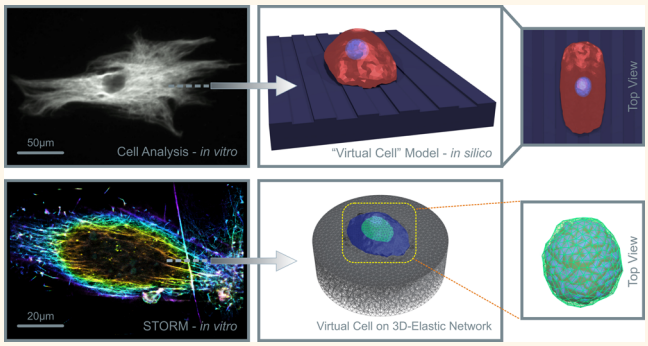


**KEYWORDS:** *micro/nanosubstrates, topography, stiffness, multicomponent cell model, virtual cell*

Physical, chemical, and mechanical properties of the extracellular matrix (ECM) in different tissues have crucial roles in directing residential cell functions.[1,2] Thanks to progress in engineering, biocompatible materials with tunable properties and patterns have been developed and employed to mimic particular ECM characteristics that control cell functions.[3] During recent years, engineered substrates (*e.g.*, with micro/nanopatterns) have been increasingly applied to trigger a range of cell functions/characteristics including cell alignment (contact guidance) and differentiation.[4] Examples include nanoscale features that direct differentiation of mesenchymal stem cells (MSCs) toward the osteoblast lineage[5]

**Received:** May 27, 2017
**Accepted:** July 24, 2017
**Published:** July 25, 2017




DOI: 10.1021/acsnano.7b03732
*ACS Nano* 2017, 11, 9084−9092

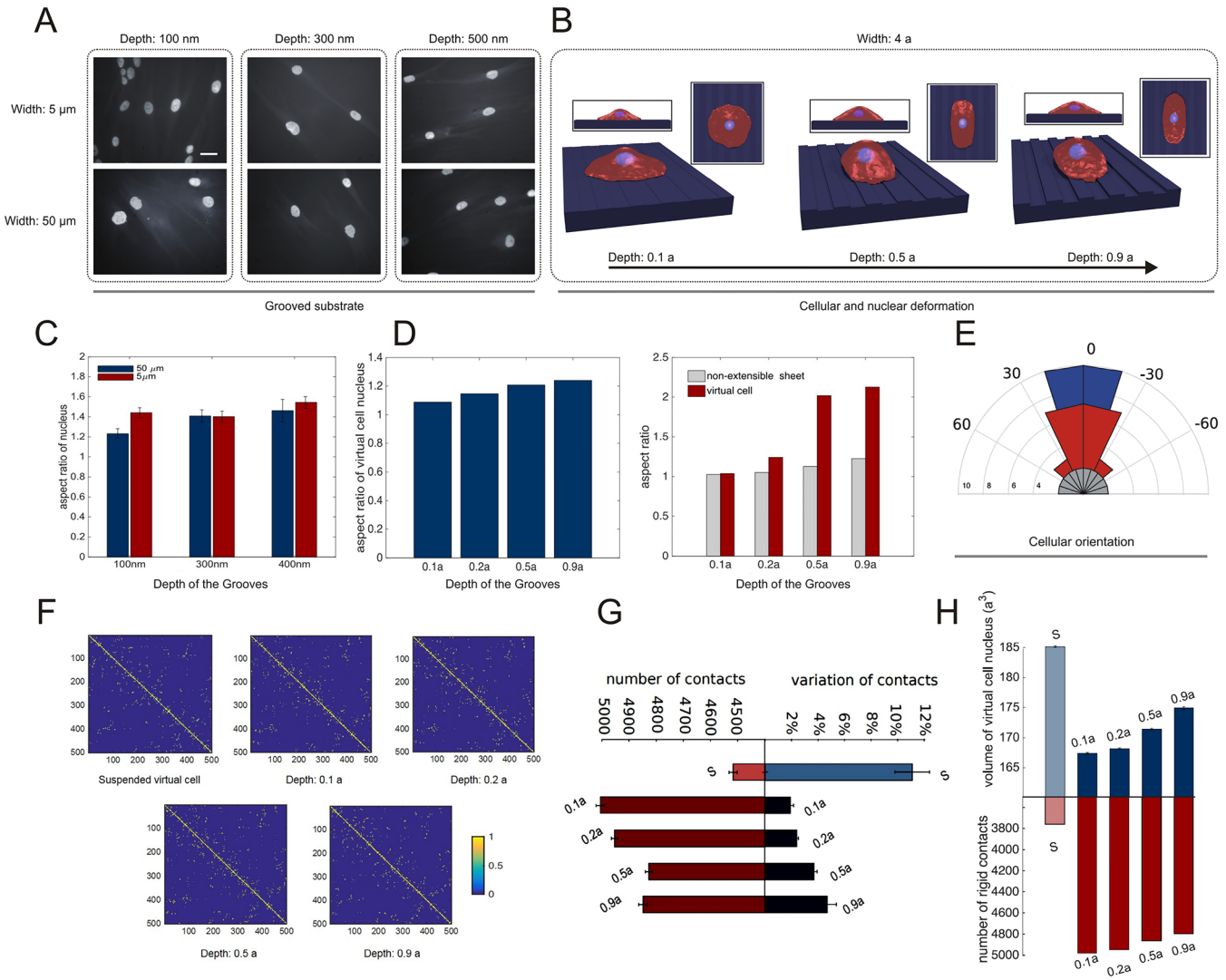


**Figure 1. Prediction of deformation and elongation of the cells on the grooved substrate using a "virtual cell modeling". (A) Cultivated cells on grooved substrates with widths of 5 and 50 $\mu$m and depths of 100−400 nm. Scale bars indicate 25 $\mu$m. (B) Morphological alteration of the virtual cell on the grooved substrate with a width of 4*a* (*i.e.*, *a* is the reduced length unit; see Methods/Experimental Section for details) and a depth of 0.1*a* − 0.9*a*. (C) Aspect ratio of the cell nucleus of the cultured cells in 50 $\mu$m (blue) and 5 $\mu$m grooves (red) *vs* the depth of the grooves (see Table S2 of the SI for details). (D) Aspect ratio of the nucleus of the "virtual cell" *vs* the depth of the grooves (left); aspect ratio of the "virtual cell" in red color and a wallpaper circular sheet with the same size of the virtual cell in gray color *vs* the depth of the grooves (right). (E) Effect of grooved substrate on the virtual cells with randomly distributed orientations. Distribution of cell orientations with regard to groove direction after placing on a flat substrate (gray), grooved substrate with a depth of 0.2*a* (red), and grooved substrate with a depth of 0.5*a* (blue). (F) Contact probability matrices of simulated chromatin fibers in equilibrium configurations of the virtual cell in suspension and on grooved substrates with different groove depth, from 0.1*a* to 0.9*a*. (G) Number of contacts (red) and the percentage of changed contacts (blue) of the virtual cell in suspension (denoted by "S") and on grooved substrates with different groove depth, from 0.1*a* to 0.9*a*. Cell absorption on the substrate increases the number of contacts and decreases the alternation of contacts during the time. (H) Volume of the virtual cell nucleus (blue) and the number of rigid contacts (red) of the virtual cell in suspension (denoted by "S") and on grooved substrates with different groove depth, from 0.1*a* to 0.9*a*. Cell absorption on the substrate decreases the volume of the nucleus and increases the number of robust contacts.**

and variation of material surface mechanical properties guiding stem cell lineage.[6]

It is clear that MSCs' function closely follows form and that the degree of cell spreading is strongly correlated to phenotype. For example, adipocytes are a low-adhesion/poorly spread MSC phenotype that produce little cytoskeletal tension.[7,8] Osteoblasts, on the other hand, are well-spread MSC derivatives with high levels of cytoskeletal tension[7−9] supported by the formation of supermature adhesions.[10] MSC phenotype itself is maintained by intermediate levels of intracellular tension and spreading, between the spreading states of fibroblasts and adipocytes.[11−13] Further, if MSCs are placed onto substrates imprinted with the morphologies of mature MSC derivative phenotypes, then they adopt those phenotypes, *e.g.*, chondrocytes. More specifically, if the cells are grown of morphological imprints of naïve stem cells, then they retain MSC phenotype for longer in culture.[4,14−16] This morphological control has generated a lot of interest in high-throughput materiomics,[17] screening technologies for chemical,[18] mechanical,[19] and topographical[20] substrate functionalizations. However, predictive modeling could also provide a powerful tool if it can be truly predictive.



DOI: 10.1021/acsnano.7b03732
*ACS Nano* 2017, 11, 9084−9092

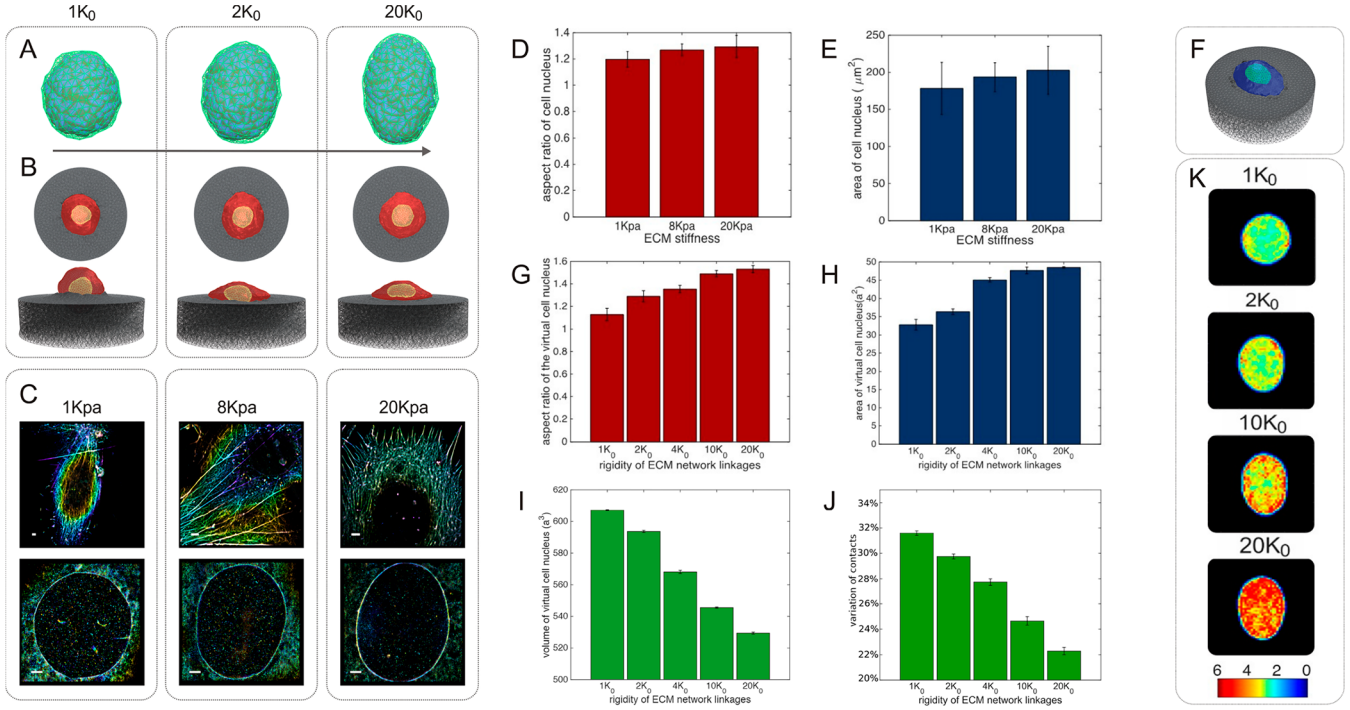


**Figure 2. Virtual cell model can predict cell/nucleus response to the ECM stiffness. (A) Resulting shapes of the nucleus of an anisotropic virtual cell on the substrates with the elastic network bond parameters of $1.0k_0$, $2.0k_0$, and $20.0\ k_0$ ($k_0$ is the parameter of elasticity in simulation units; see Methods/Experimental Section). (B) Relaxed configuration of an isotropic virtual cell on an elastic substrate. (C) Stochastic optical reconstruction microscopy (STORM) images of the cultivated cell on a polyacrylamide (PA) gel substrate with different stiffness (1, 8, and 20 kPa). Scale bars indicate 1 $\mu$m. (D) Aspect ratio of the cell nucleus *vs* the substrate stiffness in an *in vitro* study (see Table S3 of the SI for details). (E) Top view area ($\mu^2$) of the cell nucleus *vs* the substrate stiffness in an *in vitro* study (see Table S3 of the SI for details). (F) Illustrated schematic of an anisotropic virtual cell on a 3D-elastic network with a triangular top surface. (G) Aspect ratio of the anisotropic virtual cell nucleus *vs* the stiffness of the ECM substrate linkages. (H) Top view area ($a^2$) of the virtual cell nucleus *vs* the stiffness of the ECM substrate linkages. (I) Volume ($a^3$) of the virtual cell nuclei *vs* the stiffness of the ECM substrate linkages. (J) Percentage of changed chromatin contacts during the averaging *vs* the stiffness of the ECM substrate linkages. The stiffness of the ECM could affect the shape and the volume of the virtual cell nucleus and consequently the dynamics of the virtual chromatins. Statistically the chromatin contacts on stiffer ECMs are more stable than the contacts on softer ECMs. (K) Spatial density of averaged contacts between the segments of chromatin fiber for the virtual cell on an elastic substrate. The measurements of averaged contacts are performed on the horizontal cross-section of the nucleus.**

To achieve this, we developed a multicomponent cell model, the "virtual cell model", which can be used to predict cell behavior on substrates with a wide range of characteristics. The model can provide reliable information on cell, nucleus, and chromatin conformations in response to different material characteristics. The artificial cell, which we will describe, is made up from components that virtually model outer and nucleus membranes, cytoplasm and cytoskeleton, and chromatin fibers. The virtual substrate has also been developed in a way that allows it to have different morphological (topographical) and elastic characteristics. The model has the capacity not only to predict shape and conformation of the cells qualitatively but also to give quantitative results if the adequate and proper parameters are used. To show how powerful and accurate the model is, we compare the model results with the experimental readouts.

## RESULTS

**Prediction of Cell and Nucleus' Geometries on Grooved Substrates.** It is well understood that microgrooved patterns can guide cell elongation with width and depth of the grooves dictating the degree of alignment.[21] Further, it has previously been observed in elongated nuclei that signaling interactions at the nuclear membrane show an increase in activated signaling components, providing us with the shape as an indicator of "cell health".[22,23] Here, we have fabricated grooved patterns on poly(methyl methacrylate) (PMMA) substrates (Figures S1 and S2 of the Supporting Information (SI)) with various widths and depths (specifically widths of 5 and 50 $\mu$m and depths of 100, 300, and 400 nm). These parameters were selected to give the cells strong guidance cues (narrow and deep grooves) and weak guidance cues (wide and shallow grooves).[24] After culturing of the MSCs on the grooves at a seeding density of $1 \times 10^4$ cells per sample in complete media for 4 days, MSCs were fixed and stained for actin cytoskeleton and DAPI (nucleus stain) as described (Figure 1A; Figure S3 of the SI). We concomitantly experimented with the artificial cell on a model substrate to illustrate the capability of our developed model for predicting cell elongation on the grooved substrates (Figure 1). To measure elongation, we calculated the aspect ratio of the cells and nuclei by measuring the ratio of the larger to the smaller diameter of the fitted ellipses to the cell or nucleus. The results revealed that the virtual cell (see Table S1 of the SI for details on physical parameters of the model) became elongated along the grooved substrate with elongation increasing with direct proportionality to increased groove depth (see Figure 1B and Movies S1–S3 of the SI for more details).



DOI: 10.1021/acsnano.7b03732
ACS Nano 2017, 11, 9084–9092

The virtual cell also elongated along the grooves, and this led to change in nuclear morphology from spherical to ellipsoidal, which was also seen in the cell cultures (Figure 1A,B). The observed ellipsoidal shape of the nucleus is likely due to the propagation of stress from the outer membrane to the nucleus via the viscoelastic cytoskeleton and cytoplasm medium[25] (for more information see the Methods/Experimental Section). A part of the measured cell elongation, cell aspect ratio, could be caused by the effect of attachment of the cell to the vertical walls of the substrate. One may potentially counterpostulate that this is similar to elongation in visible cross-section of a "nonextensible circular wallpaper" when it covers the grooved substrate. The circular "wallpaper", after covering the grooved substrate, looks like an ellipse with the aspect ratio as a function of the depth and the width of the grooves (see Figure S1 of the SI for more information). However, the observed elongation of the virtual cell is greater than this geometrical effect, as shown in Figure 1D.

We next investigated whether the grooved substrates affect nuclear orientation. We found that the anisotropic virtual cells can adopt the shape of the substrates' grooves and thus orient along the groove direction. The degree of orientation is directly correlated to the increase in groove depth (Figure 1E).

A recent study revealed that large-scale cell shape changes have dramatic consequences on the nuclear shape and structure, resulting in a chromatin condensation.[26] This deformation in the nucleus can consequently alter the spatial configuration of the chromatin fibers and may change the cell behavior and fate.[26] To gain more insight into how chromatin reorganization may be influenced by the nuclear shape remodeling, the probability of contact between all pairs of chromatin beads (*i.e.*, fibers are modeled with bead−spring chains) in relaxed configurations is calculated and stored in contact probability matrices for the suspended virtual cell and the virtual cell on each groove depth (Figure 1F; for more information see the SI). The results show that cell attachment and elongation can change the pattern of spatial contacts between different sections of the chromatin fibers. As shown in Figure 1G and H, while increasing groove depth leads to a larger volume of the nucleus, when the suspended virtual cell (denoted by "S") is absorbed on the substrate, the volume of the nucleus significantly decreases; consequently, the number of contacts between chromatin beads increases. On the other hand, since there is less available volume inside the nucleus after absorption, the percentage of the changed contacts (see the SI for definition and more information) decreases, and as a result the number of robust (rigid) contacts increases. Briefly, the virtual cell model suggests that the cell absorption on the substrate creates more stable contacts (or exposures) between different parts of the chromatin fibers, and the strength of this effect depends on the substrate configuration.

**Cell−Substrate Stiffness Modeling Using a 3D-Elastic Network.** Cells exist in a dynamic mechanical environment where they are subject to a wide range of forces including mechanical stretching.[27,28] The interactions at the cell−ECM biointerface could trigger a range of responses that regulate cell fate. The process of sensing dynamic changes (*i.e.*, both changes in ECM stiffness and externally applied mechanical stretch) by cells is called mechanotransduction. As has been discussed, cell shape and function (*e.g.*, survival, growth, and differentiation) can be linked to substrate stiffness.[6,29−31] Understanding how cells can sense the matrix stiffness through computational 3D-modeling with simulated features will help to design optimal scaffolds to accelerate translational research in biology and tissue engineering.

Here, in order to study virtual cell response to ECM elasticity, anisotropic virtual cells (*i.e.*, virtual cells with one arbitrary preferable direction of elongation; for more information see the Methods/Experimental Section) are placed on simulated substrates with different stiffness (Figure 2A and C). Since the elastic network model is utilized for the substrate, the stiffness of the substrate depends on the elastic modulus of the network linkages, which varies from $1k_0$ to $20.0k_0$ ($k_0$ is the parameter of elasticity in simulation units; see Methods/Experimental Section). 3D-elastic networks with triangular shapes were employed to mimic a virtual cell interaction with an elastic substrate (Figure 2B and F).

Experimentally, stochastic optical reconstruction microscopy (STORM) images were employed to probe the applicability of the virtual cell model. It is noteworthy that STORM images were generated by superlocalizing the positions of $\sim 10^6$ single molecules collected over ∼50 000 frames of raw single-molecule images. The interaction of cells on polyacrylamide (PA) gel substrates with different stiffness (1, 8, and 2 kPa; see Figure S4 of the SI; these values were chosen as they are known to differentially regulate MSC fate from neural to myoblastic to osteoblastic differentiations, respectively[6,29]) was probed in terms of the effect of substrates on the cell nucleus shape. We note that the modulus of elasticity of the ECM is referred to in a biological context as stiffness. Figure 2E illustrates the nucleus spreading area on the ECM substrates and shows that a "stiffer ECM" causes an increase in nucleus spreading. Moreover, localized shape deformation of the cell nucleus is associated with an increase in substrate stiffness (Figure 2C and D). On the basis of the *in-silico* analysis, cell nucleus aspect ratio, as a measure of nucleus elongation, as well as nucleus area was observed to increase on stiffer substrates (Figure 2G and H and Movies S4 and S5).

As the consequence of elongation, the virtual cell nucleus on the stiffer ECM model had less volume (Figure 2I), as has been previously described,[20] potentially reducing the available space for chromatin inside the nucleus. As a result, the chromatin density inside the virtual nucleus and the number of contacts between chromatin segments increased in direct proportionality to reduced nuclear volume (Figure 2K). However, the modeled percentage of changes in chromatin contacts decreases on stiffer ECMs (Figure 2J). This suggests that the contacts between the chromatin segments are more stable in higher chromatin density conditions, such as with stiffer ECM. Our results provide evidence that the "virtual cell model" could be employed as a platform to understand how cells sense and respond to the ECM.

**Prediction of Stem Cell Geometry and Chromatin Conformation on Cell-Imprinted Substrates.** We have developed a platform technology of smart nanopatterned substrates. These substrates are embossed with morphologies of mature cells. In response to these morphological outlines, MSCs differentiate into the cell type represented in the imprints.[4] We have already demonstrated the success of these bioinspired cell-imprinted substrates for reliable and efficient control of MSC differentiation toward chondrocytes[15] and keratinocytes.[16] Further, we have also demonstrated that cell-patterned substrates modulate the growth (self-renewal), differentiation, and dedifferentiation of a variety of cells.[14]

To investigate the efficacy of our virtual cell approach to predict the stem cell geometry after being cultured on the



DOI: 10.1021/acsnano.7b03732
ACS Nano 2017, 11, 9084−9092

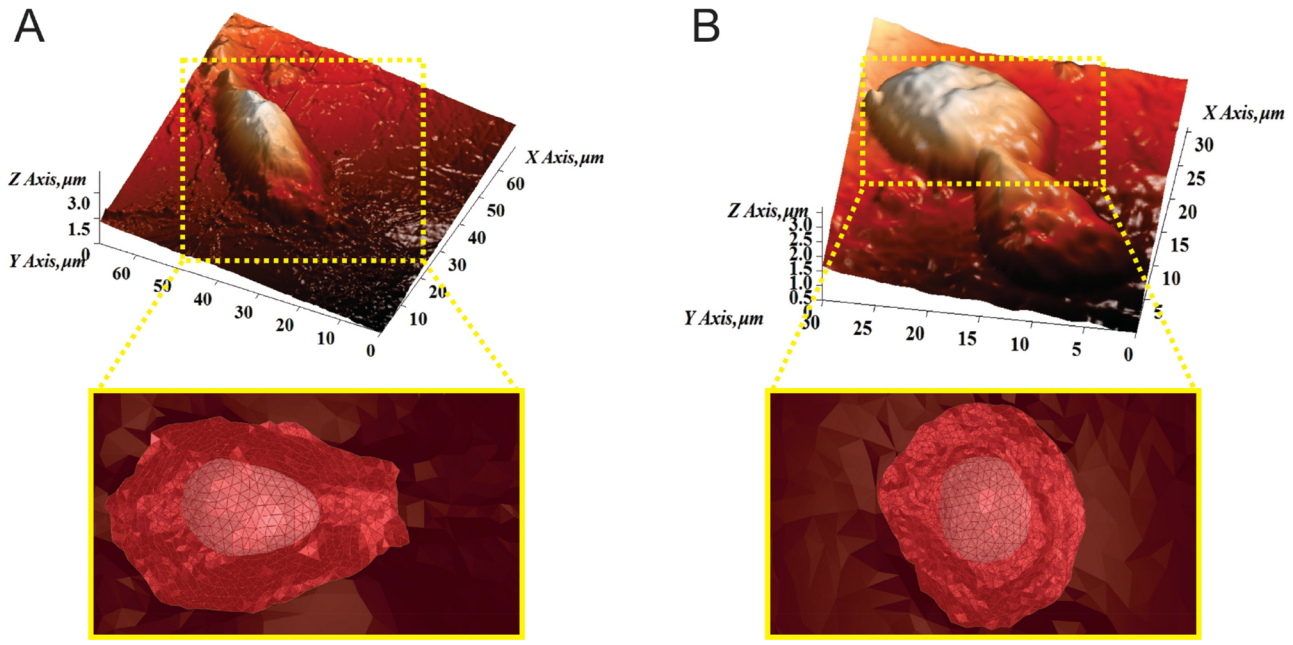


**Figure 3. Virtual cell can predict stem cell behavior on the cell-imprinted substrate. (A) Atomic-force microscopy (AFM) image showing the topography of the substrate with stem-cell-imprinted pattern (upper part) and resultant configuration of the virtual cell on the substrate with the directly adapted morphology from the stem-cell-imprinted pattern (lower part). (B) AFM image showing the topography of the substrate with keratinocyte-cell-imprinted patterns (upper part) and the resultant configuration of the virtual cell on the substrate with the directly adapted morphology from the keratinocyte-imprinted pattern (bottom). The AFM images are reproduced with permission from ref 16; American Chemical Society (2014).**

surface of cell-imprinted substrates, the morphologies of the imprinted substrates were directly captured from our published experimental data.[15,16] The resultant morphologies were then discretized into triangular elements and inserted into our model pipeline. Then, virtual cells were placed above these substrates close enough to permit attachment. The results revealed that the virtual cell could accurately predict the geometry of the cultured MSCs according to the cell type that had been used as a template (Figure 3 and Movies S5–S9). More specifically, the simulation outcomes for culturing the cells on top of imprints designed around either naïve MSCs (typically fibroblastic in appearance, Figure 3A) or dedifferentiated chondrocytes (*i.e.*, reverted to fibroblasts) (see Figure S5 of the SI for details) revealed the formation of bipolar, fibroblastic morphology and elongated nuclei, as described in the original experimental papers.[15,16] On the contrary, spherical shapes for both cell and nucleus geometry were achieved for the nanopatterend substrates with shapes of keratinocytes (Figure 3B) and chondrocytes (Figure S5 of the SI), again, in agreement with the original cell experiments.[15,16]

Numerous canonical signaling pathways are activated in response to the cellular matrix and geometric cues converging on diverse transcription factors (*e.g.*, Yes-associated protein and transcriptional coactivator with PDZ-binding domain[32]) through diverse biochemical mechanisms.[33] However, the physical transmission of such stresses through cytoplasmic–nuclear connections can remodel the chromatin structure, and this may have a more direct mechanical effect on transcription.[33] There are very few available techniques to track the chromatin conformation variations in the nucleus, including complex super-resolution microscopy[34] and Hi-C technology[35] (*i.e.*, a genome-wide method resulted from a combination of chromosome conformation capture and deep sequencing). Very recent developments in the field of super-resolution microscopy have demonstrated the close relation between the chromatin conformation and various epigenetic states.[34] Therefore, our observations on the effect of grooved substrates on the chromatin conformation perhaps suggest the significant role of surface topographies on change of gene expression, which leads to a substantial variation on the cell functions. More specifically, using the virtual cell approach, we can easily track the variation of cell and nucleus shapes together with chromatin conformational changes during differentiation. The findings should help researchers understand the mechanisms involved in shape-induced physical differentiation of stem cells.

## DISCUSSION

The crucial roles of the physicochemical properties of cell culture substrates on function and behavior of a wide range of the cells are becoming well-studied in the current literature, using experimental approaches.[2,4,5,36] However, development of *in-silico* approaches for prediction of cell responses to the physicochemical properties of substrates is still in its infancy.[37] The prediction of cell behavior, using computational approaches, could be very powerful in speeding up the design of optimal stem cell culture substrates. In this paper, we have developed a unifying computational framework and created a virtual cell model, and by correlation with experimental outcomes, we have demonstrated the capability of this model to predict cell behavior outcomes.

Our experimental examples contained substrates with different surface topographies, various mechanical properties, and cell-imprinted patterns. The shape and motility of the employed cells were controlled by both internal and external stimuli and responses of different components of the cells as they respond to topographies. Then, to produce a model that predicts the shape, deformation, conformation, and movement of the cells, we required the flexibility to model all these



DOI: 10.1021/acsnano.7b03732
*ACS Nano* 2017, 11, 9084–9092

components together. The elasticity of the membrane is also important, as cell membranes have fluidity, experience cytoskeleton and ECM forces, and also are involved in cell adhesion. Our proposed multicomponent virtual cell model demonstrated the capacity to provide all the relevant components of the cell; its outcomes were well correlated with the experimental readouts. For example, in the grooved substrates, the artificial cell accurately demonstrated the elongation in the direction of the grooved virtual substrates.

We have previously used our cell-imprinted substrates[15] to demonstrate reliable and efficient control of MSC differentiation toward chondrocytes,[15] keratinocytes,[16] and tenocytes.[14] We have also demonstrated that cell-patterned substrates modulate the differentiation, redifferentiation, and transdifferentiation of a variety of cells.[14] In this work, our goal was to probe whether the virtual cell can show the mechanism behind the observed experimental results with regard to the physical differentiation. The main hypothesis in the experimental approach was that the stem cells cultured on the cell-imprinted substrates are driven to adopt the specific shape and molecular characteristics of the mature cell types that had been used as a template for the cell-imprinting process. Our *in-silico* results verified the above hypothesis, as the virtual cell revealed that the cultured cells can mimic the shape of the imprinted substrates and change their geometry in both cellular and nuclear structures. In addition, we use our models to predict that the confining geometry of the imprints has effects on the chain arrangement of simulated chromatin fibers in the nuclei, which may have roles in the physical differentiation process. It is noteworthy that the process of cell differentiation is a complex and dynamic phenomenon; to further enhance the predictability of our virtual cell model, the model should be further improved to consider the incubation time and its effects on the differentiation process.

It is important to note that our goal in this step is to provide qualitative behavior of the MSCs. By using the real parameters (*e.g.*, Young's modulus and the force generated by actin polymerization) of a particular cell type in experiments, the model should be customized in specific cell types to provide quantitative outcomes.

## CONCLUSION

We introduced a virtual cell to probe cell function/behavior *in silico*. Using experimental results, we showed promising capability of the virtual cell to be employed as an efficient and fast high-throughput approach to provide the required information for fabrication of optimal substrates for a broad range of cellular applications. The optimal substrates, for directing specific cell function (*e.g.*, differentiation), will have translational impact through the provision of appropriate substrates to target desired stem cell phenotypes. We propose that they will find roles in prevention/prediction of diseases through better *in vitro* drug screening and through helping the cell supply chain to underpin effective cell therapy.

## METHODS/EXPERIMENTAL SECTION

**Development of the Virtual Cell.** A virtual cell model is developed to capture the cell mechanics on the substrates with different elastic properties and morphologies. The model consists of various components to simulate the outer membrane of the cell and nuclear envelope, cytoplasmic area, chromatin fibers, and extracellular matrix. A triangulated fluidic membrane is utilized to model the outer membrane of the cell and the nuclear envelope. In this model, the membrane is discretized into a triangulated mesh of vertices that are connected to each other with elastic bonds. The elastic parameters have been tuned to reflect the mechanical properties of lipid bilayers. Furthermore, membrane viscosity would be taken into account *via* the fluidity of the vertices.[38] The corresponding potential energy is given by

$$\begin{aligned} U_{\text{membrane}} &= U_{\text{bonding}} + U_{\text{repulsion}} + U_{\text{curvature}} + U_{\text{surfacearea}} \\ &= b \sum_{\langle i^{\text{v}}, j^{\text{v}} \rangle} \frac{\exp\left(\frac{1}{l_{\text{c0}} - r_{i,j}}\right)}{l_{\max} - r_{i,j}} + b \sum_{\langle i^{\text{v}}, j^{\text{v}} \rangle} \frac{\exp\left(\frac{1}{r_{i,j} - l_{\text{c1}}}\right)}{r_{i,j} - l_{\min}} \\ &+ \frac{\kappa_{\text{curve}}}{2} \sum_{\langle i^{\text{e}}, j^{\text{e}} \rangle} (1 - \cos\theta_{i,j}) + \frac{\kappa_{\text{s}}}{2}(S - S_0)^2 \end{aligned} \tag{1}$$

where $U_{\text{bonding}}$ and $U_{\text{repulsion}}$ are the bonding and repulsive potentials, respectively, which limit the bond length to be in the range of $[l_{\min}, l_{\max}]$. In the first and second terms, the summation is over all connected vertices ($\langle i^{\text{V}}, j^{\text{V}} \rangle$) and $r_{i,j}$ denotes the distance between neighboring vertices. Here, we use $b = 80k_{\text{B}}T$, $l_{\max} = 1.33a$, $l_{\min} = 0.67a$, $l_{\text{c0}} = 1.15a$, and $l_{\text{c1}} = 0.85a$, where $a$ is the initial triangle edge length.[38] Local curvature and its fluctuations are controlled by bending energy $U_{\text{curvature}}$, in the third term, the summation is over all neighboring triangular elements ($\langle i^{\text{e}}, j^{\text{e}} \rangle$), $\theta_{i,j}$ is the angle between the two normal vectors of neighboring elements, and $\kappa_{\text{curve}} = 20k_{\text{B}}T$ is the curvature energy constant. The surface area of membranes is kept constant during the simulations through constraint energy on the surface area $U_{\text{surface area}}$ with $\kappa_{\text{s}} = 1\frac{k_{\text{B}}T}{a^4}$.

The cell membrane geometry is initially considered spherical, and the nucleus membrane geometry is set the same as the cell membrane, with a smaller volume. The potential energy introduced in eq 1 is applied to both the cell and nucleus membranes.

The cytoplasm and cytoskeleton network are modeled by a network of distributed mass particles, which fill the space between the nucleus and the cell membrane. These particles are interconnected, and they are also connected to one-fourth of membrane nodes through Voigt and Maxwell fractional viscoelastic elements.[39,40] The network topology is captured by a three-dimensional tetrahedral mesh,[41] and the potential energy of the network is given as

$$U_{\text{cyt}} = \frac{\kappa_{\text{cyt}}}{2} \sum_{\langle i,j \rangle} u_{i,j} = \frac{\kappa_{\text{cyt}}}{2} \sum_{\langle i,j \rangle} (|r_i - r_j| - r_{i,j}^{\text{e}})^2 \tag{2}$$

The sum is over all connected vertices, $\kappa_{\text{cyt}}$ is the stiffness of the linkages and is set to be $\frac{k_{\text{B}}T}{a^2} \equiv \kappa_0$, $u_{i,j}$ is the potential energy of the linkage between the $i^{\text{th}}$ and the $j^{\text{th}}$ mass particles, and $r_i$ and $r_j$ are the corresponding position vectors. The equilibrium length of elements ($r_{i,j}^{\text{e}}$) is not fixed and evolves dynamically in viscous response to mechanical stress with the following relations:

$$\frac{\mathrm{d}r_{i,j}^{\text{e}}}{\mathrm{d}t} = \frac{f_{i,j}}{\mu_0} \tag{3}$$

$$f_{i,j} = -\frac{\mathrm{d}u_{i,j}}{\mathrm{d}r} \tag{4}$$

where $f_{i,j}$ is the value of the generated force between the $i^{\text{th}}$ and the $j^{\text{th}}$ mass particles and $\mu_0$ is the viscous coefficient of the network. The cytoplasm mass particles are not allowed to penetrate into the cell and nucleus membranes.

The chromatin fibers are confined in the nucleus. We used a bead–spring model with excluded volume interaction to simulate the fibers. The interacting potentials of the chromatin fibers consisting of $N_{\text{c}}$ chains are



DOI: 10.1021/acsnano.7b03732
ACS Nano 2017, 11, 9084–9092

$$U_{\text{chains}} = U_{\text{bond}} + U_{\text{bending}} + U_{\text{excluded volume}}$$
$$= \frac{\kappa_{\text{bonding}}}{2} \sum_{i=1}^{N_c} \sum_{j=1}^{N_i-1} (r_{j,j+1}^{i} - r_0)^2 + \frac{\kappa_{\text{bending}}}{2} \sum_{i=1}^{N_c} \sum_{j=1}^{N_i-2} (\theta_{j,j+1}^{i} - \theta_0)^2$$
$$+ \sum_{\substack{\langle i,j \rangle \\ i<j, r_{ij}<\sigma_{\text{ch}}}} 4 \in_{\text{ch}} \left\{ \left( \frac{\sigma_{\text{ch}}}{r_{ij}} \right)^{12} - \left( \frac{\sigma_{\text{ch}}}{r_{ij}} \right)^{6} \right\} \quad (5)$$

where $N_i$ represents the number of beads of the $i^{\text{th}}$ chain. $\kappa_{\text{bonding}}$ and $\kappa_{\text{bending}}$ are bond and bending stiffness. $r_{j,j+1}^{i}$ and $\theta_{j,j+1}^{i}$ are the bond length and the bond angle, respectively. The equilibrium bond length and angle are respectively set to $r_0 = 2\sigma_{\text{ch}}$ and $\theta_0 = 0$. In the third term, only the repulsive part of the Lennard-Jones potential is considered for each pair of beads. The length and the depth of the potential are given by $\sigma_{\text{ch}}$ and $\in_{\text{ch}}$, respectively. The nuclear envelope is impenetrable for the chains.

To model the ECM, we employed an elastic network model whose top surface is triangulated[40] (this is similar to the cytoskeleton−cytoplasm model having equal mesh size). The mechanical characteristics of the substrate are specified by the elasticity of the linkages $\kappa_{\text{ECM}}$, and there are two possible ways of interaction between the cell and the top surface of the ECM: (1) Depending on the mechanical and chemical properties of the cell membrane, the cell is able to adhere on the substrate.[42,43] (2) Due to the activity and polymerization of the actin network at the cell periphery, the cell membrane is able to spread on the substrate.[44−46] The adhesion of the cell membrane to the substrate is modeled through a generic potential such that when the membrane elements are close enough to the substrate elements, they interact through the following Lennard-Jones potential:

$$u_{\text{L-J}}^{i,j} = 4 \in_{\text{ECM}} \left\{ \left( \frac{\sigma_\perp}{d_\perp^{i,j}} \right)^{10} - \left( \frac{\sigma_\perp}{d_\perp^{i,j}} \right)^{4} \right\} \quad (6)$$

Here $d^{i,j}{}_\perp$ is the shortest distance between the center of the $i^{\text{th}}$ membrane element and the $j^{\text{th}}$ surface element (see Supporting Information), and the depth and the length of the Lennard-Jones potential are given by $\in_{\text{ECM}}$ and $\sigma_\perp$, respectively.

To model the outward pushing force applied to the membrane by the polymerization of the actin network at the cell periphery, we used an effective force $F_{\text{active}}$, whose alignment is parallel to the local curvature vector of the membrane. This force pushes the membrane elements from where they are located to within a distance of $a + \sigma_\perp$ from the substrate elements. Because the physical sources of $F_{\text{active}}$ are internal, $F_{\text{active}}$ should not impose any net force to the cell by its own; therefore, after applying $F_{\text{active}}$ to the corresponding membrane elements, the inverse of the net generated force is distributed between all membrane nodes.

Additionally, the structural and mechanical characteristics of the cytoplasm of some specific cells (polarized cells) induce anisotropy to them when they are spreading on the ECM.[47,48] To include such substantive elongation anisotropy of the cell, one arbitrary direction on the ECM substrate is chosen such that along this direction the magnitude of the $F_{\text{active}}$ is higher than other directions. Consequently, this enables the virtual cell to spread on the substrate anisotropically.

To perform the simulations, the virtual cell model is implemented as an integrated program *via* the C++ platform. In all simulations, the chromatin chains are initially confined in a spherical volume within the radius of the nucleus and then are placed inside the nucleus. The elastic network of the cytoplasm and cytoskeleton consists of (locally connected) mass particles; the network is also connected to one-fourth of the nodes of the cell and the nucleus membrane. Putting all elements together, we let the cell be relaxed by looking at the energy and the force distributions at constant temperature $T$. It takes about 100 000 simulation steps until the system equilibrates. Then we place the cell on the substrate and wait the same time before reporting the cells' configurations. Chromatin conformations are averaged over the intervals of 10 000 simulation steps.

## ASSOCIATED CONTENT

### Supporting Information

The Supporting Information is available free of charge on the ACS Publications website at DOI: 10.1021/acsnano.7b03732.

Additional characterization of the substrates, cells, and virtual cell model including confocal microscopy, STORM, and SEM (PDF)
Simulation movies (AVI)
(AVI)
(AVI)
(AVI)
(AVI)
(AVI)
(AVI)
(AVI)
(AVI)

## AUTHOR INFORMATION


### Corresponding Authors

*E-mail: mmahmoudi@bwh.harvard.edu.
*E-mail: ejtehadi@sharif.edu.

### ORCID

Maziar Heidari: 0000-0002-8081-6602
Michal Wojcik: 0000-0002-0053-1018
Ke Xu: 0000-0002-2788-194X
Morteza Mahmoudi: 0000-0002-2575-9684


### Notes

The authors declare no competing financial interest.

## ACKNOWLEDGMENTS

M.W. acknowledges support from the NSF Graduate Research Fellowship under DGE 1106400. K.X. acknowledges support from Packard Fellowships for Science and Engineering. M.J.D. acknowledges support from Biotechnology and Biological Sciences Research Council (BBSRC), grant BB/G008868/1. M.M. acknowledges support from National Institute for Medical Research Development (NIMAD) 942893.

## REFERENCES

(1) Sutherland, R. M. Cell and Environment Interactions in Tumor Microregions: The Multicell Spheroid Model. *Science* **1988**, *240*, 177−184.
(2) Dalby, M. J.; Gadegaard, N.; Oreffo, R. O. Harnessing Nanotopography and Integrin-Matrix Interactions to Influence Stem Cell Fate. *Nat. Mater.* **2014**, *13*, 558−569.
(3) Stevens, M. M.; George, J. H. Exploring and Engineering the Cell Surface Interface. *Science* **2005**, *310*, 1135−1138.
(4) Mashinchian, O.; Turner, L.-A.; Dalby, M. J.; Laurent, S.; Shokrgozar, M. A.; Bonakdar, S.; Imani, M.; Mahmoudi, M. Regulation of Stem Cell Fate by Nanomaterial Substrates. *Nanomedicine* **2015**, *10*, 829−847.
(5) Dalby, M. J.; Gadegaard, N.; Tare, R.; Andar, A.; Riehle, M. O.; Herzyk, P.; Wilkinson, C. D.; Oreffo, R. O. The Control of Human Mesenchymal Cell Differentiation Using Nanoscale Symmetry and Disorder. *Nat. Mater.* **2007**, *6*, 997−1003.
(6) Engler, A. J.; Sen, S.; Sweeney, H. L.; Discher, D. E. Matrix Elasticity Directs Stem Cell Lineage Specification. *Cell* **2006**, *126*, 677−689.


DOI: 10.1021/acsnano.7b03732
*ACS Nano* 2017, 11, 9084−9092

(7) McBeath, R.; Pirone, D. M.; Nelson, C. M.; Bhadriraju, K.; Chen, C. S. Cell Shape, Cytoskeletal Tension, and RhoA Regulate Stem Cell Lineage Commitment. *Dev. Cell* **2004**, *6*, 483−495.
(8) Kilian, K. A.; Bugarija, B.; Lahn, B. T.; Mrksich, M. Geometric Cues for Directing the Differentiation of Mesenchymal Stem Cells. *Proc. Natl. Acad. Sci. U. S. A.* **2010**, *107*, 4872−4877.
(9) Yim, E. K.; Pang, S. W.; Leong, K. W. Synthetic Nanostructures Inducing Differentiation of Human Mesenchymal Stem Cells into Neuronal Lineage. *Exp. Cell Res.* **2017**, *313*, 1820−1829.
(10) Biggs, M. J.; Richards, R. G.; Gadegaard, N.; Wilkinson, C. D.; Oreffo, R. O.; Dalby, M. J. The Use of Nanoscale Topography to Modulate the Dynamics of Adhesion Formation in Primary Osteoblasts and ERK/MAPK Signalling in STRO-1+ Enriched Skeletal Stem Cells. *Biomaterials* **2009**, *30*, 5094−5103.
(11) Dalby, M. J.; Gadegaard, N.; Oreffo, R. O. Harnessing Nanotopography and Integrin-Matrix Interactions to Influence Stem Cell Fate. *Nat. Mater.* **2014**, *13*, 558−569.
(12) Tsimbouri, P. M.; McMurray, R. J.; Burgess, K. V.; Alakpa, E. V.; Reynolds, P. M.; Murawski, K.; Kingham, E.; Oreffo, R. O.; Gadegaard, N.; Dalby, M. J. Using Nanotopography and Metabolomics to Identify Biochemical Effectors of Multipotency. *ACS Nano* **2012**, *6*, 10239−10249.
(13) Lee, L. C.; et al. Nanotopography Controls Cell Cycle Changes Involved with Skeletal Stem Cell Self-Renewal and Multipotency. *Biomaterials* **2017**, *116*, 10−20.
(14) Bonakdar, S.; et al. Cell-Imprinted Substrates Modulate Differentiation, Redifferentiation, and Transdifferentiation. *ACS Appl. Mater. Interfaces* **2016**, *8*, 13777−13784.
(15) Mahmoudi, M.; Bonakdar, S.; Shokrgozar, M. A.; Aghaverdi, H.; Hartmann, R.; Pick, A.; Witte, G.; Parak, W. J. Cell-Imprinted Substrates Direct the Fate of Stem Cells. *ACS Nano* **2013**, *7*, 8379−8384.
(16) Mashinchian, O.; Bonakdar, S.; Taghinejad, H.; Satarifard, V.; Heidari, M.; Majidi, M.; Sharifi, S.; Peirovi, A.; Saffar, S.; Taghinejad, M. Cell-Imprinted Substrates Act as an Artificial Niche for Skin Regeneration. *ACS Appl. Mater. Interfaces* **2014**, *6*, 13280−13292.
(17) Celiz, A. D.; Smith, J. G.; Langer, R.; Anderson, D. G.; Winkler, D. A.; Barrett, D. A.; Davies, M. C.; Young, L. E.; Denning, C.; Alexander, M. R. Materials for Stem Cell Factories of the Future. *Nat. Mater.* **2014**, *13*, 570−579.
(18) Mei, Y.; et al. Combinatorial Development of Biomaterials for Clonal Growth of Human Pluripotent Stem Cells. *Nat. Mater.* **2010**, *9*, 768−778.
(19) Gobaa, S.; Hoehnel, S.; Roccio, M.; Negro, A.; Kobel, S.; Lutolf, M. P. Artificial Niche Microarrays for Probing Single Stem Cell Fate in High Throughput. *Nat. Methods* **2011**, *8*, 949−955.
(20) Unadkat, H. V.; et al. An Algorithm-Based Topographical Biomaterials Library to Instruct Cell Fate. *Proc. Natl. Acad. Sci. U. S. A.* **2011**, *108*, 16565−16570.
(21) Yim, E. K.; Reano, R. M.; Pang, S. W.; Yee, A. F.; Chen, C. S.; Leong, K. W. Nanopattern-Induced Changes in Morphology and Motility of Smooth Muscle Cells. *Biomaterials* **2005**, *26*, 5405−5413.
(22) Rangamani, P.; Lipshtat, A.; Azeloglu, E. U.; Calizo, R. C.; Hu, M.; Ghassemi, S.; Hone, J.; Scarlata, S.; Neves, S. R.; Iyengar, R. Decoding Information in Cell Shape. *Cell* **2013**, *154*, 1356−1369.
(23) Dahl, K. N.; Ribeiro, A. J.; Lammerding, J. Nuclear Shape, Mechanics, and Mechanotransduction. *Circ. Res.* **2008**, *102*, 1307−1318.
(24) Dalby, M. J.; McCloy, D.; Robertson, M.; Wilkinson, C. D.; Oreffo, R. O. Osteoprogenitor Response to Defined Topographies with Nanoscale Depths. *Biomaterials* **2006**, *27*, 1306−1315.
(25) Kumar, S.; Maxwell, I. Z.; Heisterkamp, A.; Polte, T. R.; Lele, T. P.; Salanga, M.; Mazur, E.; Ingber, D. E. Viscoelastic Retraction of Single Living Stress Fibers and Its Impact on Cell Shape, Cytoskeletal Organization, and Extracellular Matrix Mechanics. *Biophys. J.* **2006**, *90*, 3762−3773.
(26) Versaevel, M.; Grevesse, T.; Gabriele, S. Spatial Coordination Between Cell and Nuclear Shape Within Micropatterned Endothelial Cells. *Nat. Commun.* **2012**, *3*, 671.
(27) Li, J.; Han, D.; Zhao, Y.-P. Kinetic Behaviour of the Cells Touching Substrate: The Interfacial Stiffness Guides Cell Spreading. *Sci. Rep.* **2015**, *4*, 3910.
(28) Mullen, C. A.; Vaughan, T. J.; Billiar, K. L.; McNamara, L. M. The Effect of Substrate Stiffness, Thickness, and Cross-Linking Density on Osteogenic Cell Behavior. *Biophys. J.* **2015**, *108*, 1604−1612.
(29) Engler, A. J.; Griffin, M. A.; Sen, S.; Bönnemann, C. G.; Sweeney, H. L.; Discher, D. E. Myotubes Differentiate Optimally on Substrates with Tissue-Like Stiffness Pathological Implications for Soft or Stiff Microenvironments. *J. Cell Biol.* **2004**, *166*, 877−887.
(30) Guilak, F.; Cohen, D. M.; Estes, B. T.; Gimble, J. M.; Liedtke, W.; Chen, C. S. Control of Stem Cell Fate by Physical Interactions With the Extracellular Matrix. *Cell Stem Cell* **2009**, *5*, 17−26.
(31) Khetan, S.; Guvendiren, M.; Legant, W. R.; Cohen, D. M.; Chen, C. S.; Burdick, J. A. Degradation-Mediated Cellular Traction Directs Stem Cell Fate in Covalently Crosslinked Three-Dimensional Hydrogels. *Nat. Mater.* **2013**, *12*, 458−465.
(32) Yang, C.; Tibbitt, M. W.; Basta, L.; Anseth, K. S. Mechanical Memory and Dosing Influence Stem Cell Fate. *Nat. Mater.* **2014**, *13*, 645−652.
(33) Wang, N.; Tytell, J. D.; Ingber, D. E. Mechanotransduction at a Distance: Mechanically Coupling the Extracellular Matrix With the Nucleus. *Nat. Rev. Mol. Cell Biol.* **2009**, *10*, 75−82.
(34) Boettiger, A. N.; Bintu, B.; Moffitt, J. R.; Wang, S.; Beliveau, B. J.; Fudenberg, G.; Imakaev, M.; Mirny, L. A.; Wu, C.-t.; Zhuang, X. Super-Resolution Imaging Reveals Distinct Chromatin Folding for Different Epigenetic States. *Nature* **2016**, *529*, 418−422.
(35) Lieberman-Aiden, E.; Van Berkum, N. L.; Williams, L.; Imakaev, M.; Ragoczy, T.; Telling, A.; Amit, I.; Lajoie, B. R.; Sabo, P. J.; Dorschner, M. O. Comprehensive Mapping of Long-Range Interactions Reveals Folding Principles of The Human Genome. *Science* **2009**, *326*, 289−293.
(36) McMurray, R. J.; Gadegaard, N.; Tsimbouri, P. M.; Burgess, K. V.; McNamara, L. E.; Tare, R.; Murawski, K.; Kingham, E.; Oreffo, R. O.; Dalby, M. J. Nanoscale Surfaces for the Long-Term Maintenance of Mesenchymal Stem Cell Phenotype and Multipotency. *Nat. Mater.* **2011**, *10*, 637−644.
(37) Albert, P. J.; Schwarz, U. S. Dynamics of Cell Ensembles on Adhesive Micropatterns: Bridging the Gap Between Single Cell Spreading and Collective Cell Migration. *PLoS Comput. Biol.* **2016**, *12*, e1004863.
(38) Noguchi, H.; Gompper, G. Dynamics of Fluid Vesicles in Shear Flow: Effect of Membrane Viscosity and Thermal Fluctuations. *Phys. Rev. E* **2005**, *72*, 011901.
(39) Schiessel, H.; Metzler, R.; Blumen, A.; Nonnenmacher, T. Generalized Viscoelastic Models: Their Fractional Equations with Solutions. *J. Phys. A: Math. Gen.* **1995**, *28*, 6567−6584.
(40) Lewandowski, R.; Chorążyczewski, B. Identification of the Parameters of the Kelvin−Voigt and the Maxwell Fractional Models, Used to Modeling of Viscoelastic Dampers. *Comput. Struct.* **2010**, *88*, 1−17.
(41) Geuzaine, C.; Remacle, J. F. Gmsh: A 3-D Finite Element Mesh Generator With Built-In Pre-and Post-Processing Facilities. *Int. J. Numer. Method. Biomed. Eng.* **2009**, *79*, 1309−1331.
(42) Gruhn, T.; Lipowsky, R. Temperature Dependence of Vesicle Adhesion. *Phys. Rev. E* **2005**, *71*, 011903.
(43) Sackmann, E. Biological Membranes Architecture and Function. In *Structure and Dynamics of Membranes: I. From Cells to Vesicles/II. Generic and Specific Interactions*; Lipowsky, R.; Sackmann, E., Eds.; Elsevier: North Holland, 1998; pp 1−64.
(44) Fletcher, D. A.; Mullins, R. D. Cell Mechanics and The Cytoskeleton. *Nature* **2010**, *463*, 485−492.
(45) Schwarz, U. S.; Safran, S. A. Physics of Adherent Cells. *Rev. Mod. Phys.* **2013**, *85*, 1327−1381.
(46) Parsons, J. T.; Horwitz, A. R.; Schwartz, M. A. Cell Adhesion: Integrating Cytoskeletal Dynamics and Cellular Tension. *Nat. Rev. Mol. Cell Biol.* **2010**, *11*, 633−643.


DOI: 10.1021/acsnano.7b03732
*ACS Nano* 2017, 11, 9084−9092

(47) Zemel, A.; Rehfeldt, F.; Brown, A.; Discher, D.; Safran, S. Optimal Matrix Rigidity for Stress-Fibre Polarization in Stem Cells. *Nat. Phys.* **2010**, *6*, 468−473.
(48) Hu, S.; Eberhard, L.; Chen, J.; Love, J. C.; Butler, J. P.; Fredberg, J. J.; Whitesides, G. M.; Wang, N. Mechanical Anisotropy of Adherent Cells Probed by a Three-Dimensional Magnetic Twisting Device. *Am. J. Physiol. Cell Physiol.* **2004**, *287*, C1184−C1191.



DOI: 10.1021/acsnano.7b03732
*ACS Nano* 2017, 11, 9084−9092